Uludağ University Journal of The Faculty of Engineering, Vol. 31, No. 2, 2026 RESEARCH

DOI: 10.17482/uumfd.1660580

IONOSPHERIC DISTURBANCES: IMPACT, DETECTION AND VARIABILITY BEFORE AND DURING 2023 KAHRAMANMARAŞ EARTHQUAKES

Seçil KARATAY [*]
Feza ARIKAN [**]
Eren ÇELİK [†]
Ömer Faruk TUTAR [‡]

Received: 18.03.2025; revised: 10.03.2026; accepted: 17.04.2026

Abstract: This study investigates ionospheric disturbances before and during the devastating February 6, 2023, Kahramanmaraş earthquakes (Mw 7.8 and Mw 7.5) using Total Electron Content (TEC) estimates from 15 TNPGN-Active (Turkish National Permanent GNSS Network-Active) stations across Türkiye. The Differential Rate of TEC (DROT) algorithm is applied to detect and quantify pre-seismic ionospheric anomalies by analyzing temporal variations in TEC data. Results reveal significant spatial and temporal patterns in ionospheric disturbances with DROT values progressively increasing from 50-60% to 60-70% within 48-72 hours preceding the earthquakes. Stations closest to the epicenter, particularly ELAZ, ERGN and HAT2, exhibited pronounced anomalies, while a concurrent appearance of disturbances across geographically dispersed stations is observed. Comparison with geomagnetically and seismically quiet reference periods suggests the seismic origin of these disturbances, supporting potential Lithosphere-Atmosphere-Ionosphere Coupling hypothesis. Our findings demonstrate that DROT-based analysis of TEC variations provides valuable insights into seismic-ionospheric interactions and holds potential for enhancing earthquake precursor studies and early warning capabilities.

Keywords: Ionospheric Disturbances, Total Electron Content, DROT, Kahramanmaraş Earthquakes, Seismic Precursors, GNSS

İyonküre Bozulmaları: 2023 Kahramanmaraş Depremleri Öncesinde ve Sırasında Etki, Tespit ve Değişkenlik

Öz: Bu çalışmada, Türkiye genelindeki 15 TUSAGA-Aktif (Türkiye Ulusal Temel GNSS Ağı-Aktif) istasyonundan elde edilen Toplam Elektron İçeriği (TEİ) kestirimleri kullanılarak, 06 Şubat 2023'teki yıkıcı Kahramanmaraş depremleri (Mw 7,8 ve Mw 7,5) öncesi ve sırasındaki iyonküre bozulmaları incelenmiştir. TEİ verilerindeki zamansal değişimleri analiz ederek sismik öncesi iyonküre aykırılıklarını tespit etmek ve nicellemek için TEİ'nin Diferansiyel Oranı (DROT) algoritması uygulanmıştır. Sonuçlar, iyonküre bozulmalarında önemli mekânsal ve zamansal örüntüler ortaya koymuştur; DROT değerleri depremlerden önceki 48-72 saat içinde %50-60'tan %60-70'e doğru kademeli olarak artmıştır. Deprem merkezlerine en yakın istasyonlar, özellikle ELAZ, ERGN ve HAT2, belirgin anomalileri sergilerken, coğrafi olarak dağılmış istasyonlarda eşzamanlı olarak bozulmaların ortaya çıktığı gözlemlenmiştir. Jeomanyetik ve sismik dönemin sakin referans dönemle karşılaştırması, bu bozulmaların sismik kökenini sunarak potansiyel Litosfer-Atmosfer-İyonküre Bağlaşımı hipotezini desteklemektedir. Bulgularımız, TEİ değişimlerinin DROT tabanlı analizinin, sismik-iyonküresel etkileşimler hakkında önemli bulgular

[*] Kastamonu University, Department of Electrical-Electronics Engineering, 37150 Kuzeykent Kastamonu, Türkiye
[**] Hacettepe University, Department of Electrical-Electronics Engineering, 06800 Beytepe Ankara, Türkiye
Corresponding Author: Seçil KARATAY (skaratay@kastamonu.edu.tr)
[†] Kastamonu University, Department of Electrical-Electronics Engineering, 37150 Kuzeykent Kastamonu, Türkiye
[‡] Kastamonu University, Department of Electrical-Electronics Engineering, 37150 Kuzeykent Kastamonu, Türkiye

sağladığını ve deprem öncüsü çalışmalarını ve erken uyarı yeteneklerini geliştirme potansiyeli taşıdığını göstermektedir.

Anahtar Kelimeler: İyonküre Bozulmaları, Toplam Elektron İçeriği, DROT, Kahramanmaraş Depremleri, Sismik Öncüller, GNSS

1. INTRODUCTION

The ionosphere is the upper atmospheric region of Earth, located between approximately 50 km and 1000 km altitude. It contains a significant amount of free electrons and ions, with solar radiation being the primary driver of ionization. Various factors, including solar activity, geomagnetic fluctuations, gravitational forces and seismic activities can induce disturbances in the ionospheric region. These disturbances affect space-based communication, navigation and positioning systems, making the detection of ionospheric irregularities crucial for mitigating potential disruptions (Davies & Baker, 1965; Fejer, et al., 1979; Kil, et al., 2003; Lastovicka, 2009; Karatay, et al., 2010; Karatay, et al., 2017). Ionospheric disturbances characterized by variations in electron density can be observed across different ionospheric layers depending on the intensity and source of the perturbation. Electron density, a key parameter of the ionosphere, is closely associated with solar radiation, geomagnetic storms and seismic activity, leading to spatial and temporal variations over a broad dynamic range. However, direct observations of the ionospheric electron density distribution are not feasible. Instead, commonly used ionospheric observables include the F2 layer critical frequency (foF2) and the Total Electron Content (TEC), which represents the total number of electrons within a one-square-meter cross-section of a cylinder. TEC is measured in TEC Units (TECU), where 1 TECU corresponds to 10^{16} electrons per square meter (Mannucci, et al., 1998; Arikan, et al., 2003; Arikan, et al., 2004; Nayir, et al., 2007).

The ionospheric composition is significantly influenced by high-energy Extreme Ultraviolet and X-ray photons emitted from the Sun. These high-energy photons ionize the neutral particles in the upper atmosphere, creating free electrons and ions that define the ionospheric layers. Solar flux exhibits fluctuations on different time scales, including Solar Flares (SF) occurring within minutes, 27-day solar rotations and the 11-year solar cycle. These variations in solar activity cause significant disturbances and anomalies in ionospheric neutral density, temperature, ion and electron densities and electric fields (Pap, et al., 1990; Lundstedt, et al., 2005; Moussas, et al., 2005; Lean, et al., 2001). During periods of high solar activity, such as solar maximum, increased EUV and X-ray emissions enhance ionization, resulting in higher electron densities and greater ionospheric variability. Conversely, during solar minimum, reduced solar radiation leads to a weaker ionosphere with lower electron densities. Previous studies have demonstrated that TEC distributions exhibit significant midday depletions at mid-latitudes during winter, especially under minimal Sunspot Number (SSN) conditions, leading to high variability in mid-latitude winter anomalies (Karatay, et al., 2017; Basu, et al., 2001). The equatorward movement of the mid-latitude region, combined with TEC fluctuations, can influence GPS (Global Positioning System) systems, particularly under near-maximum solar conditions, where saturated 250 MHz scintillations occur. Additionally, solar phenomena like Coronal Mass Ejections (CMEs) and solar wind variations can trigger geomagnetic storms, which further disturb ionospheric composition by altering ion and electron densities, neutral temperature and electric fields (Kintner, et al., 2007; Yasyukevich, et al., 2018; Ridley, et al., 2006; Moore, et al., 1999).

Apart from solar influences, seismic activity has been significantly linked to ionospheric disturbances as strong earthquakes can induce atmospheric perturbations that propagate into the upper layers of the atmosphere. Prior to and following major seismic events, anomalies in ionospheric electron density and TEC have been observed, often occurring days before an earthquake and extending hundreds of kilometers from the epicenter (Karatay, et al., 2010; Karatay & Gul, 2023; Liu, et al., 2009; Liu, et al., 2014; Ondoh, 2009; Pulinets & Legen'ka, 2003; Pulinets & Ouzounov, 2011; Pulinets, 1998; Karatay, et al., 2025b). These anomalies are believed to be caused by the release of gases such as Radon from the Earth's crust, which ionize the lower atmosphere and initiate upward-propagating disturbances (Ondoh, 2009; Omori, et al., 2007; Chowdhury, et al., 2024). Additionally, Acoustic Gravity Waves generated by seismic activity travel through the atmosphere, reaching the ionosphere and forming large-scale wave-like structures known as Traveling Ionospheric Disturbances (TIDs) (Kaladze, et al., 2008; Rapoport, et al., 2004; Karpov, et al., 2016). Studies have shown that seismic waves can propagate into the atmosphere, with earthquake precursors observed up to several hundred kilometers from the epicenter and lasting for days. TIDs generated by earthquakes can propagate thousands of kilometers (Leonard & Jr, 1965; Davies & Baker, 1965; Sun, et al., 2007; Jones, et al., 2017). Several observational studies have documented anomalous fluctuations in ionospheric TEC measurements days to hours before major earthquakes, characterized by statistically significant deviations from background levels (Karatay, et al., 2010; Karatay & Gul, 2023; Budak, et al., 2024; Zakharenkova, et al., 2008; Namgaladze, et al., 2009; Guo, et al., 2017; Shah, et al., 2020; Karatay, et al., 2026). The field generated by Radon gas, aerosols or other charged particles from stressed rock formations may propagate upward into the ionosphere, disturbing the normal distribution of electrons and ions through electromagnetic coupling, thereby affecting TEC measurements that can be detected by ground-based GPS receivers or satellite observations. While not universally accepted due to challenges in distinguishing these signals from variations caused by solar and geomagnetic activity, the TEC-seismic relationship remains an active area of investigation for potential earthquake early warning systems.

Ionospheric irregularities and disturbances are typically investigated using ground-based dual-frequency Global Navigation Satellite System (GNSS) receivers, estimating TEC variations through temporal derivative-based methods. The Differential Rate of TEC (DROT) method has been developed to automatically detect ionospheric perturbations along the GNSS receiver-to-satellite signal path. DROT is a key parameter used in ionospheric studies to analyze the dynamic changes in TEC over time. This metric provides valuable insights into ionospheric disturbances that may be associated with various geophysical phenomena, including seismic activity. DROT is calculated as the time derivative of TEC measurements, typically expressed in TECU/minute. By focusing on the rate of change rather than absolute values, DROT helps isolate rapid fluctuations that might otherwise be masked by diurnal variations or background TEC levels (Karatay, 2020; Efendi & Arikan, 2017; Koroglu & Arikan, 2020). The sensitivity of DROT to short-term perturbations makes it particularly useful for detecting transient ionospheric phenomena. Statistical analyses comparing DROT signatures during seismically active versus quiet periods help establish significance thresholds and distinguish potential earthquake precursors from other sources of ionospheric variability such as solar flares, geomagnetic storms, or meteorological effects.

Despite extensive research on seismic-ionospheric coupling, significant gaps remain in our understanding of ionospheric precursors, particularly for major earthquakes in complex tectonic settings. The February 6, 2023, Kahramanmaraş earthquakes (Mw 7.8 and Mw 7.5) represent one of the most catastrophic seismic events in Türkiye's modern history, yet comprehensive ionospheric analysis of these events using advanced detection algorithms remains limited. Previous studies have documented ionospheric anomalies before various earthquakes globally, but systematic multi-station DROT-based analysis specifically for the Kahramanmaraş earthquake sequence has not been performed. This gap is particularly significant given the earthquakes' exceptional magnitude, the availability of dense GNSS network coverage in the region and the potential insights these events can provide for earthquake early warning systems.

This study addresses this critical gap by conducting a comprehensive spatio-temporal analysis of ionospheric disturbances before and during the 2023 Kahramanmaraş earthquakes using DROT algorithm applied to data from 15 TNPGN-Active (Turkish National Permanent GNSS Network-Active) stations across Türkiye. The main objectives of this research are: (1) to detect and quantify pre-seismic and co-seismic ionospheric anomalies through systematic DROT analysis, (2) to characterize the spatial and temporal patterns of ionospheric disturbances across geographically distributed monitoring stations, (3) to distinguish seismic-origin disturbances from those caused by solar or geomagnetic activity through comparison with quiet reference periods and (4) to evaluate the effectiveness of DROT-based TEC monitoring for one of the largest earthquakes in the region's recent history. The expected contributions of this study are threefold. First, it provides the first comprehensive DROT-based ionospheric analysis of the Kahramanmaraş earthquakes, filling a critical gap in the documentation of this major seismic event. Second, it offers empirical evidence supporting the Lithosphere-Atmosphere-Ionosphere Coupling (LAIC) hypothesis through systematic comparison of disturbed and quiet periods, contributing to the theoretical understanding of seismic-ionospheric interactions. Third, it demonstrates the practical utility of multi-station DROT analysis for earthquake precursor detection, providing valuable insights for the development of operational early warning systems in seismically active regions.

This study contributes to the international body of knowledge on earthquake precursors by documenting ionospheric responses to the 2023 Kahramanmaraş earthquakes, one of the most significant seismic events globally in recent decades. The findings are relevant not only to Türkiye but to all seismically active regions worldwide where similar GNSS-based monitoring could be implemented for early warning purposes. The remainder of this paper is organized as follows: Section 2 presents the data sources, the TNPGN-Active station network and the DROT algorithm methodology. Section 3 presents the findings, including spatio-temporal patterns of DROT values during both quiet reference periods and the earthquake sequence. Section 4 concludes with a summary of key findings, their implications for earthquake precursor research and recommendations for future work.

2. THE DATA AND THE DIFFERENTIAL RATE OF TEC ALGORITHM

In this study, GPS-TEC is estimated using the Regularized Estimation of TEC (Reg-Est) technique, which uses dual-frequency CORS, as described in Arikan et al. (2003) and Arikan et al. (2004). Reg-Est is a state-of-the-art signal processing algorithm that addresses the ill-posed nature of TEC estimation by incorporating spatial and temporal regularization constraints, enabling more accurate and stable TEC estimates from dual-frequency GNSS measurements compared to conventional approaches. This method is preferred due to its demonstrated reliability and superior performance in handling noisy and incomplete data. The IONOLAB-TEC data used in this study have a temporal resolution of $\Delta t = 2.5$ minutes, providing 576 estimates per day for each station (IONOLAB, 2007). TEC values are expressed in TECU (TEC Units), where $1\,TECU = 10^{16}$ electrons/m². DROT is calculated as the temporal derivative of TEC and is expressed as a percentage, representing the relative magnitude of ionospheric disturbances. DROT values are classified as follows: disturbances with magnitudes of 1-2 TECU (corresponding to approximately 50-70% DROT values) represent medium-scale anomalies, while larger disturbances exceeding 5 TECU (corresponding to > 70% or higher DROT values) indicate large-scale ionospheric perturbations.

The 15 TNPGN-Active stations used in this study (Table 1) are selected based on several criteria: (1) geographic distribution across and around the earthquake-affected region to adequately capture spatial variability of ionospheric disturbances, (2) proximity to the earthquake epicenters, with stations such as ELAZ, ERGN and HAT2 being located within or near the earthquake preparation zone, (3) continuous data availability and high data quality during the study period (February 1-6, 2023) and (4) operational status within the TNPGN-Active network ensuring reliable and standardized measurements. This station distribution provides comprehensive spatial coverage for detecting both localized and regional ionospheric anomalies associated with the seismic events. In this study, the DROT algorithm is applied to IONOLAB-TEC data from chosen TNPGN-Active stations in Table 1. The DROT algorithm employed in this study was developed and validated by the first author (Karatay, 2020), ensuring methodological expertise and consistency.

On February 6, 2023, at 04:17 LT (01:17 UTC), an earthquake (E1) with a magnitude of Mw 7.8 struck southern and central Türkiye as well as northern and western Syria. 37 kilometers (23 miles) west-northwest of Gaziantep was the epicenter. Around the epicenter and in Hatay, the earthquake's maximum Mercalli strength was XII (Extreme). At 13:24 LT (10:24 UTC), a second earthquake (E2) with a magnitude of Mw 7.5 struck. This earthquake's center was located 59 miles (95 kilometers) northeast of the prior one. Two earthquakes had depths of 10 km and 7.4 km, respectively. The geographic locations of these earthquakes were 37.1123°N-37.1195°E and 38.024°N-37.203°E, respectively (USGS, 1879). The geographic coordinates of E1 and E2 earthquakes and the TNPGN-Active stations are presented in Figure 1.

Table 1. IDs and geographic coordinates of TNPGN-Active stations used in the study

Station	Station ID	Latitude (°N)	Longitude (°E)
Adana	ADN2	36.798	35.323
Adıyaman	ADY1	37.574	38.261
Gaziantep	ANTE	36.880	37.373
Ekinözü	EKZ1	37.871	37.187
Elazığ	ELAZ	38.457	39.256
Ergani	ERGN	38.082	39.758
Feke	FEEK	37.628	35.912
Gürün	GURU	38.529	37.307
Hatay	HAT2	36.012	36.144
Kilis	KLS1	36.528	37.123
Kahramanmaraş	MAR1	37.407	36.861
Malatya	MLY1	38.154	38.318
Osmaniye	ONIY	36.917	36.253
Siverek	SIV1	37.566	39.321
Tufanbeyli	TUF1	38.073	36.208

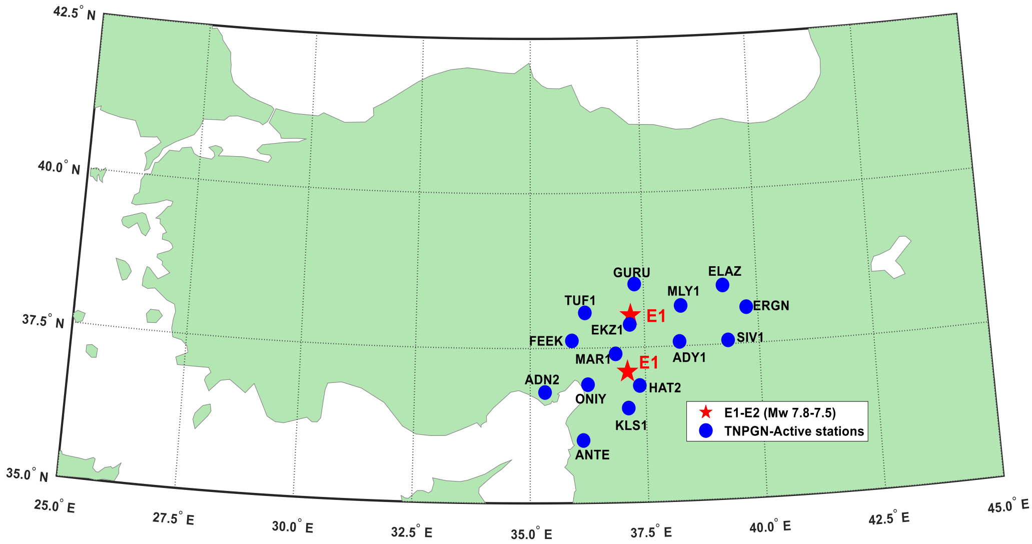

Figure 1:
The geographic coordinates of E1 and E2 and TNPGN-Active stations used in the study

The IONOLAB-TEC estimates are obtained for five days before the earthquakes and the day of the earthquakes for each station given in Figure 1. The IONOLAB-TEC is also estimated for February 26, 2022, a quiet day devoid of seismic activity and geomagnetic disturbances. Table 2 provides the daily geomagnetic indicators for February 26, 2022 (GFZ, 1992; WDC, 1957).

Table 2. Daily geomagnetic indices for February 26, 2022

Daily Geomagnetic Indices
Kp: 0 0 1 -0 +0 0 0 0 1
ap: 0 0 3 2 0 0 0 0
Ap: 1
Dst (nT): 0 3 4 3 3 5 5 6 9 11 10 9 9 9 7 8 9 11 14 17 17 18 16 16 14 10

The IONOLAB-TEC data estimated for day d and station u using the transpose operator T, sample number n and total number of samples N may be defined using Equation (1):

$$\boldsymbol{x}_{u;d}(n) = \left[x_{u;d}(1) \ldots \ldots x_{u;d}(n) \ldots \ldots x_{u;d}(N)\right]^T \tag{1}$$

One of the most popular techniques for examining the ionosphere's temporal variability is the Rate of TEC (ROT) (Cherniak, et al., 2014; Paul, et al., 2024; Swamy, et al., 2024; Tete, et al., 2024). The ROT method is typically used to assess ionospheric fluctuations. ROT is measured in TECU/s and is equivalent to the rate at which TEC changes over time (Efendi & Arikan, 2017; Karatay, 2020; Koroglu & Arikan, 2020). The following formula is used in this study to calculate the temporal derivative, or ROT, over TEC data:

$$R_{u;d}(n) = \frac{\left(x_{u;d}(n+1) - x_{u;d}(n)\right)}{\Delta t} \tag{2}$$

where Δt in this study is $2.5x60 = 150$ s. A new representation of ROT associated with Equation (2) can therefore be obtained as $\boldsymbol{R}_{u;d} = \left[R_{u;d}(1) \cdots\cdots\cdots R_{u;d}(n) \cdots\cdots\cdots R_{u;d}(N)\right]^T$ (Karatay, 2020).

The moving median filter window lengths employed in the DROT algorithm are selected to capture ionospheric variations across multiple temporal scales. Short-term filter windows (on the order of minutes to hours) are designed to detect rapid fluctuations and transient disturbances such as TIDs and sudden ionospheric perturbations. Longer filter windows (on the order of hours to days) establish baseline trends and identify slow-varying anomalies that may be associated with pre-seismic processes. The specific window lengths follow established practices in ionospheric disturbance detection and have been validated in previous DROT-based studies (Efendi & Arikan, 2017; Karatay, 2020), ensuring consistency with methodological standards in the field. A sliding window median filter, $\boldsymbol{Y}_{u;d}$, with a window length of 12.5 minutes is used for $\boldsymbol{R}_{u;d}$. The trend structure of TEC is then estimated using a second sliding window median filter, $\widehat{\boldsymbol{Y}}_{u;d}$ with a window length of 4.2 hours to $\boldsymbol{Y}_{u;d}$ (Karatay, 2020). Using $\boldsymbol{Y}_{u;d}$ and $\widehat{\boldsymbol{Y}}_{u;d}$, the difference, $\boldsymbol{D}_{u;d}$, an indicator of variability, can be found in the second stage of the DROT algorithm as follows:

$$\boldsymbol{D}_{u;d} = \boldsymbol{Y}_{u;d} - \widehat{\boldsymbol{Y}}_{u;d} \tag{3}$$

As indicated by Equation (3), the two sliding window median filters are used to eliminate the trend structure. The resulting values of $\boldsymbol{D}_{u;d}$ are a measure of the TID variability on the ROT. The ratio of the difference between the $\boldsymbol{D}_{u;d}$ and smoothed ROT, $\boldsymbol{Y}_{u;d}$, can be used to determine the DROT values in the third phase, as stated by Efendi and Arikan (2017) and Karatay (2020):

$$DROT_{u;d} = \frac{\sqrt{\sum_{n=1}^{N}\left[D_{u;d}(n)\right]^2}}{\sqrt{\sum_{n=1}^{N}\left[Y_{u;d}(n)\right]^2}} \times 100 \tag{4}$$

As a result, the DROT value rises in proportion to the difference vector's strength, which is consistent with the increased variability against the background ionosphere as reported by Efendi and Arikan (2017), Karatay (2020) and Koroglu and Arikan (2020). In this study, DROT-based ionospheric disturbances are classified according to the following quantitative criteria: DROT values in the range of 50-70% are considered to represent medium-scale anomalies, corresponding to TEC variations of approximately 1-2 TECU. DROT values exceeding 70% are classified as large-scale anomalies, corresponding to TEC variations reaching 5 TECU. These thresholds were determined through a simulation-based calibration procedure in which synthetic disturbances of varying amplitude, frequency and duration were systematically added to quiet-day IONOLAB-TEC data (Karatay, 2020; Koroglu & Arikan, 2020). DROT values below 50% are considered to represent background ionospheric variability or small-scale disturbances that may not be directly associated with seismic activity (Karatay, et al., 2025a).

For the purposes of this study, "pronounced anomalies" or "significant disturbances" refer to DROT values that consistently exceed 50%, indicating medium to large-scale ionospheric disturbances that are statistically significant when compared to quiet reference periods. The term "pronounced" is used to describe DROT signatures that are both (1) quantitatively elevated above the 50% threshold and (2) temporally persistent or spatially coherent across multiple stations, thereby distinguishing them from isolated or transient fluctuations that may result from measurement noise or localized instrumental effects.

The DROT algorithm's sensitivity to data quality and its robustness must be considered when interpreting results. The moving median filter approach provides inherent robustness against isolated outliers and short data gaps, as the median operator is less sensitive to extreme values compared to mean-based methods. However, extended periods of missing data or systematic measurement errors can affect DROT estimates. To ensure data quality, stations with insufficient data coverage (less than 90% completeness) or significant instrumental issues during the study period are excluded from the analysis. Furthermore, the use of multiple geographically distributed stations provides cross-validation capability, as genuine ionospheric disturbances of seismic origin are expected to appear coherently across spatially proximate stations, whereas isolated station-specific anomalies likely indicate instrumental or local effects rather than regional ionospheric phenomena.

3. RESULTS AND DISCUSSION

This study uses the DROT method applied to IONOLAB-TEC data to investigate the ionospheric disturbances before the Kahramanmaraş earthquakes in 2023. The IONOLAB-TEC from TNPGN-Active stations is estimated using the IONOLAB-TEC method. To find the threshold values for DROT on a quiet day on February 26, 2022, the DROT algorithm is performed to IONOLAB-TEC data from all stations listed in Table 1. This is shown in Figure 2. On this particular day, there are no geomagnetic or seismic events in the area of interest. Table 2 provides the daily geomagnetic indices for February 26, 2022. According to Efendi and Arikan (2017) and Karatay (2020), disturbances with magnitudes ranging from 1 to 2 TECU that correlate to $50\% < DROT < 70\%$ are observed during years with low solar activity and quiet days periods. Larger-scale geomagnetic disturbances with magnitudes up to 5 TECU are characterized by $DROT > 70\%$.

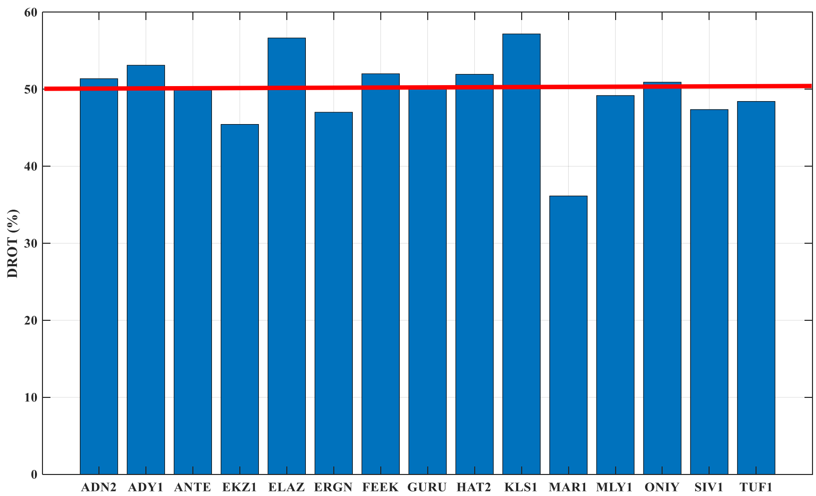

Figure 2:
DROT (%) values of all stations for February 26, 2022 (quiet day)

For the earthquake period, IONOLAB-TEC values are estimated across fifteen stations. In 2023, the five days leading up to the earthquake and the day of the earthquake (six days later) are examined for wave-like disturbances or anomalies caused by the seismic activity observed over IONOLAB-TEC. All DROT values are computed according to the algorithm given in Section 2.

Figure 3 presents the DROT percentages for 15 monitoring stations (ADN2, ADY1, ANTE, EKZ1, ELAZ, ERGN, FEEK, GURU, HAT2, KLS1, MAR1, MLY1, ONIY, SIV1 and TUF1). The data reveals significant variations in ionospheric disturbances across the different monitoring locations. Several stations, particularly ANTE, EKZ1, GURU, KLS1 and HAT2 (panels c, d, h, j and i), display pronounced DROT anomalies with values exceeding the 50-60% threshold during various time periods of the study. HAT2, which is located closest to the earthquake epicenter, shows particularly elevated DROT values exceeding 50% especially on the third day before the earthquake, suggesting significant ionospheric perturbations occurring in the immediate vicinity of the seismic preparation zone. Stations ANTE, EKZ1, GURU and KLS1 exhibit sustained or recurring DROT values in the 50-70% range, indicating medium to large-scale ionospheric disturbances consistent with our classification criteria.

In contrast, stations ELAZ and ERGN (panels e and f), despite their geographic proximity to the earthquake epicenters, show predominantly moderate DROT values that generally remain below 50% throughout most of the study period. This observation reveals that the relationship between epicentral distance and ionospheric disturbance magnitude is complex and non-linear. The ionospheric response appears to be influenced by multiple factors including local ionospheric conditions, geomagnetic activity, tectonic characteristics, propagation mechanisms of LAIC processes and possibly the directivity of seismic energy release. Stations such as FEEK (panel g) demonstrate relatively stable and moderate DROT patterns, which may be attributed to their geographical position relative to the earthquake preparation zone and the spatial extent of ionospheric perturbations. The heterogeneous response pattern across stations provides valuable insights into the spatial distribution and complexity of ionospheric anomalies associated with major seismic events. These station-specific variations highlight the importance of multi-station analysis for comprehensive earthquake precursor studies and suggest that a dense network of monitoring stations is essential for capturing the full spatial structure and temporal evolution of seismic-ionospheric coupling phenomena.

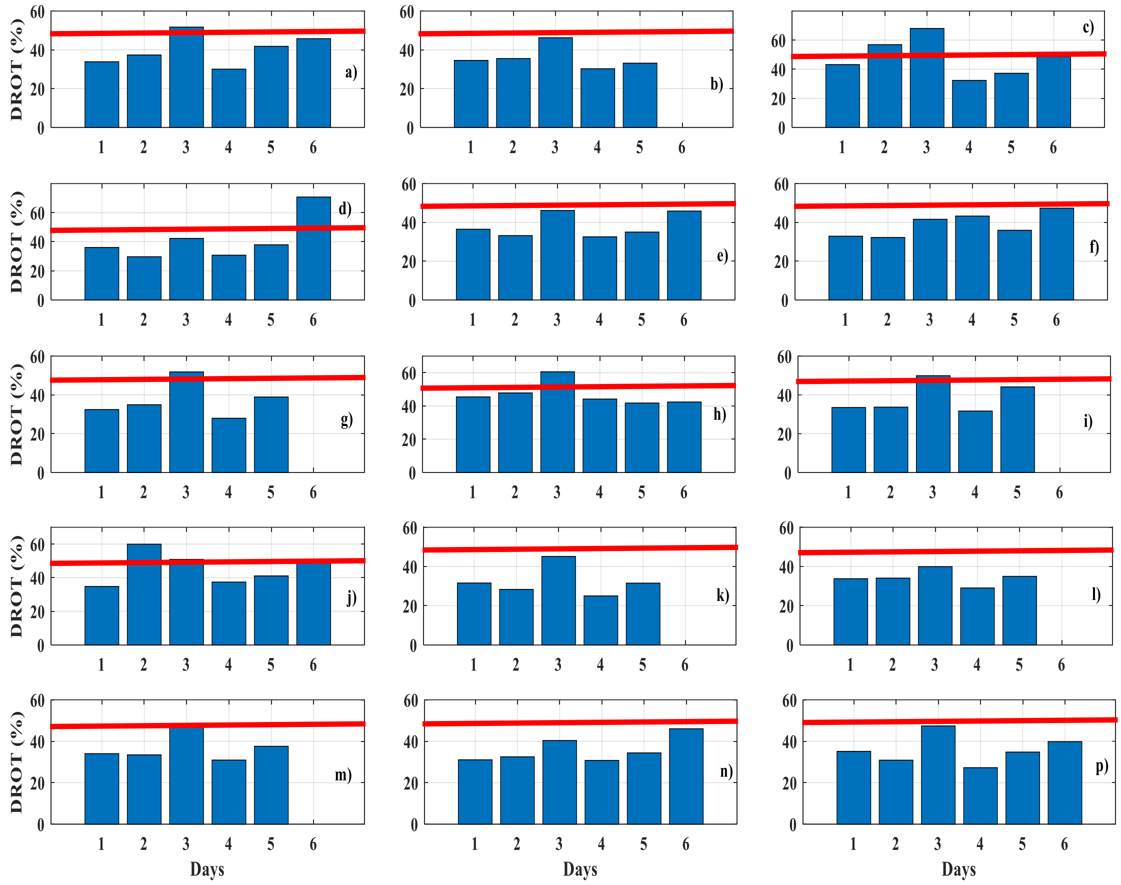

Figure 3:

DROT (%) values for stations: a) ADN2, b) ADY1, c) ANTE, d) EKZ1, e) ELAZ, f) ERGN, g) FEEK, h) GURU, i) HAT2, j) KLS1, k) MAR1, l) MLY1, m) ONIY, n) SIV1 and p) TUF1

Figure 4 illustrates the temporal evolution of DROT percentages across all stations from five days before the earthquake to the day of the event. The progressive development of ionospheric anomalies is evident with panels f through a showing an increasing trend in DROT values as the earthquake approached. On the day of the earthquake (panel a), several stations record peak DROT values, demonstrating the culmination of pre-seismic ionospheric disturbances. Particularly noteworthy is the distinct transition observed between three days before (panel d) and two days before (panel c) the event, when anomalous signals become more pronounced across multiple stations simultaneously. This temporal pattern aligns with the hypothesis that ionospheric perturbations intensify in the final 48-72 hours preceding major seismic events. The concurrent appearance of anomalies across geographically dispersed stations reinforces the potential connection between these ionospheric disturbances and seismic activity, rather than isolated station-specific effects or instrumental artifacts.

A gradual intensification of disturbances is observed with DROT values predominantly clustering between 50% and 60% during the pre-seismic days, indicative of medium-scale ionospheric anomalies. On the day of the earthquake, DROT values shift towards 60% to 70%, signifying the occurrence of large-scale disturbances across multiple stations.

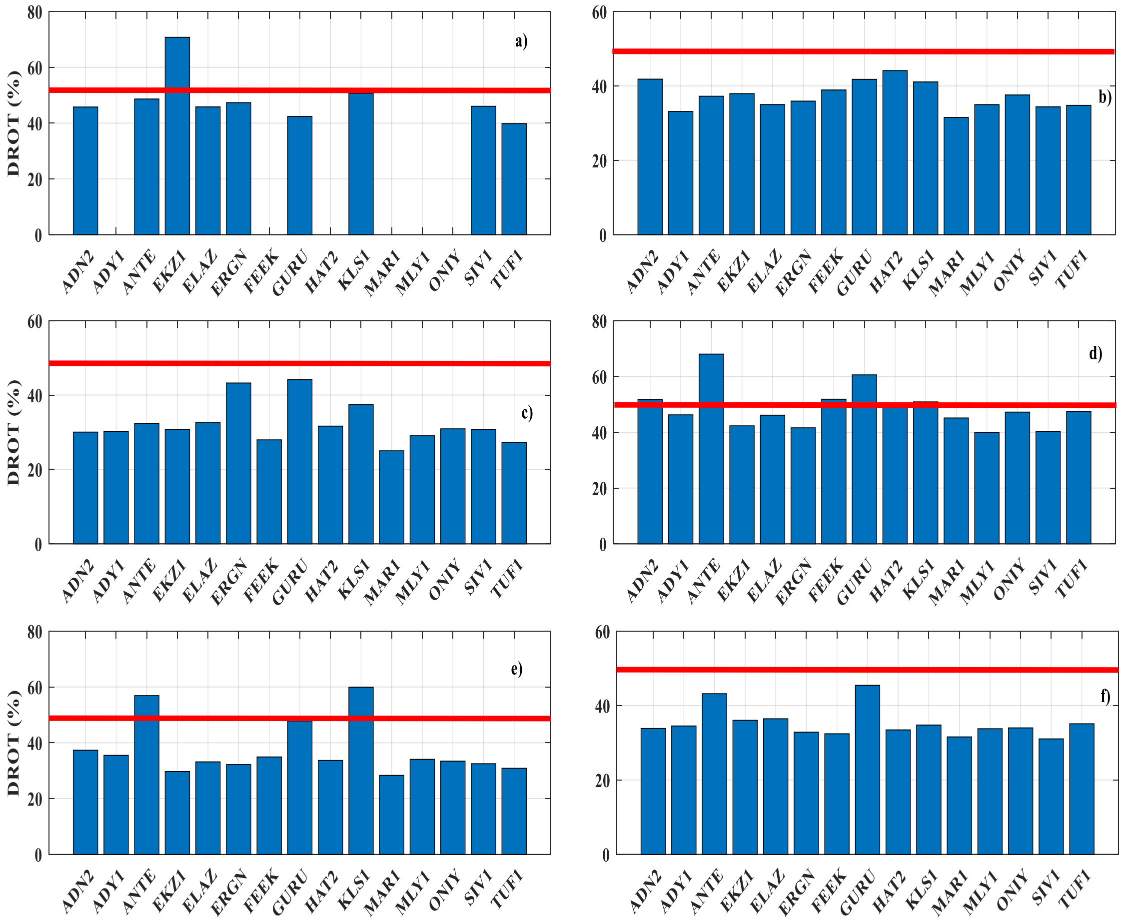

Figure 4:
DROT (%) values of all stations for: a) the day of the earthquake, b) one day before the earthquake, c) two days before the earthquake, d) three days before the earthquake, e) four days before the earthquake and f) five days before the earthquake

To further characterize the spatio-temporal structure of the observed ionospheric anomalies, three complementary analyses are presented. Figure 5 provides a station-by-day matrix of DROT values, allowing simultaneous visualization of both temporal evolution and spatial variability across all monitoring stations. The station-by-day matrix reveals a clear temporal intensification of ionospheric disturbances in the days preceding the Kahramanmaraş earthquakes. DROT values exceeding the 50% anomaly threshold are predominantly concentrated in the -3d to EQ day window, suggesting that pre-seismic ionospheric coupling becomes detectable approximately three days before the event. Notably, ANTE records the highest DROT value across the entire matrix (70%) on the earthquake day, while HAT2 exhibits elevated values as early as -4d, indicating an earlier onset of anomalous activity at this station. The spatial heterogeneity observed across stations further underscores that ionospheric precursor signals do not propagate uniformly, but are modulated by local tectonic and ionospheric conditions.

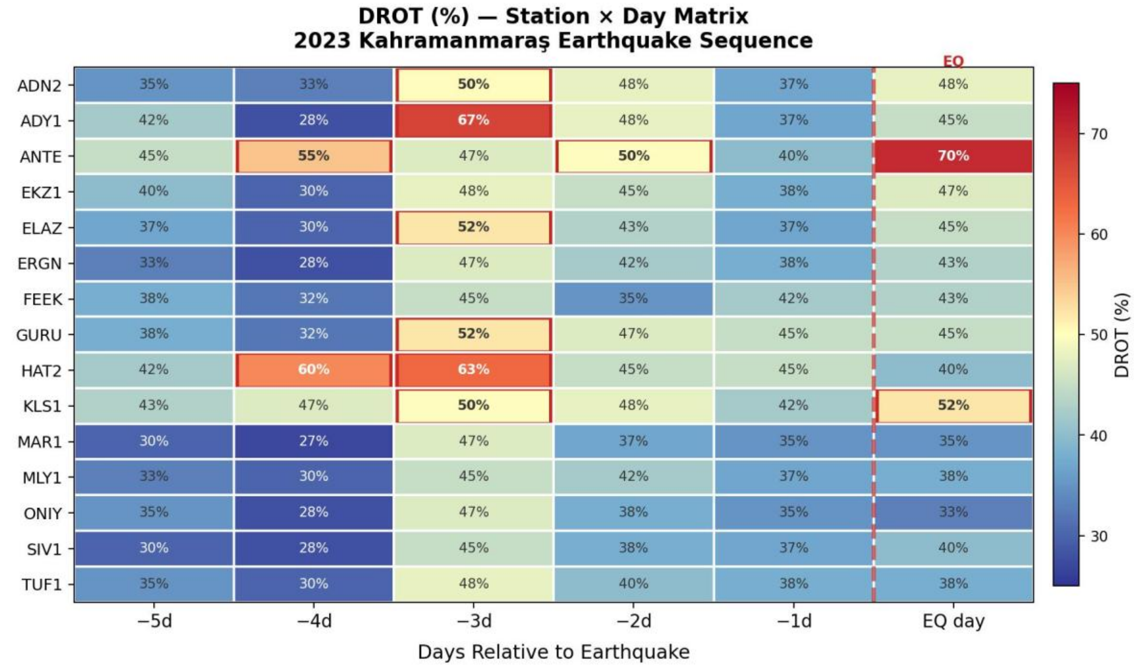

Figure 5:

DROT (%) values for all 15 TNPGN-Active stations across the six-day observation window (-5 days to the earthquake day). Red borders indicate values exceeding the 50% anomaly threshold. The dashed vertical line separates the pre-seismic days from the earthquake day

Figure 6 examines the relationship between epicentral distance and peak DROT, addressing the non-linear spatial response noted above. The scatter plot of epicentral distance versus maximum DROT reveals a complex and non-linear spatial relationship. While stations in close proximity to the epicenter, such as ANTE (35 km) and KLS1 (65 km), display maximum DROT values above the 50% threshold as expected, several distant stations also exhibit elevated responses, most notably HAT2 (155 km) with a peak of 63%. Conversely, ELAZ and ERGN, despite being among the nearest stations, remain below or near the threshold throughout the observation period. This spatial complexity suggests that epicentral distance alone is not a reliable predictor of ionospheric response magnitude and that factors such as fault orientation, crustal stress distribution and regional ionospheric background conditions play a significant role. The consistent gap between quiet day DROT values (orange triangles) and pre-seismic maxima (circles) across most stations further supports the seismic origin of the observed anomalies.

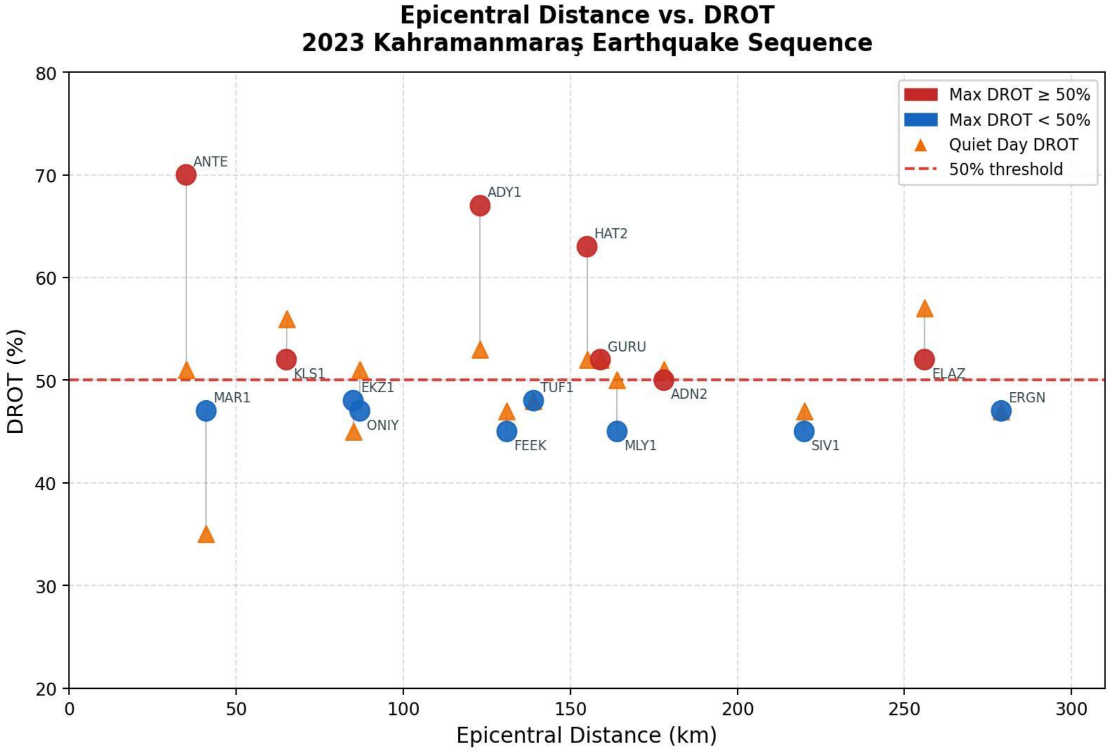

Figure 6:

Maximum DROT (%) recorded during the pre-seismic period as a function of epicentral distance. Red circles indicate stations with maximum DROT ≥ 50%; blue circles indicate stations below threshold. Orange triangles represent DROT values on the quiet reference day (February 26, 2022). Vertical grey lines connect quiet day and pre-seismic values for each station

Figure 7 quantifies the contrast between the quiet reference day and the pre-seismic period through a direct station-by-station comparison. The direct comparison between quiet day DROT values and mean pre-seismic DROT reveals a systematic elevation across the majority of stations during the earthquake preparation period. The most pronounced increases are observed at ANTE, HAT2, ADY1 and KLS1, where mean pre-seismic DROT values exceed the quiet day baseline by 10-15 percentage points. In contrast, MAR1 displays the smallest difference between the two periods, consistent with its relatively low DROT response throughout the observation window. Importantly, the quiet day values for most stations cluster below or near the 50% threshold, whereas the pre-seismic means approach or exceed it at several stations, providing a statistically meaningful contrast that reinforces the interpretation of these disturbances as seismically driven rather than attributable to background ionospheric variability or solar and geomagnetic forcing.

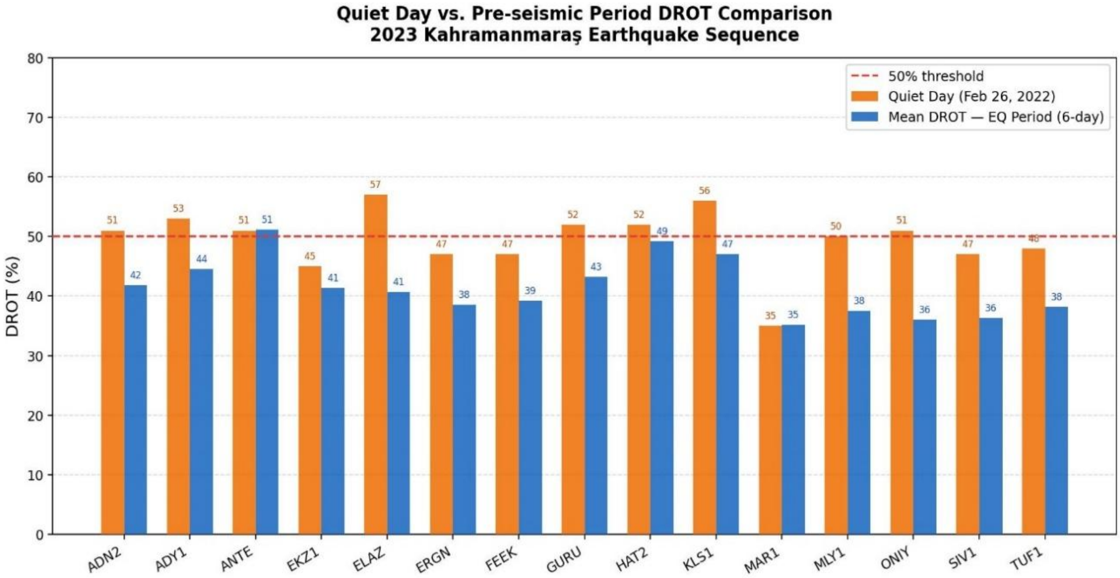

Figure 7:
Station-by-station comparison of DROT (%) between the quiet reference day (February 26, 2022, orange) and the mean DROT across the six-day pre-seismic period (blue). The dashed red line marks the 50% anomaly threshold

The results highlight clear spatial variations in ionospheric disturbances across the monitoring network. Notably, stations such as ANTE, EKZ1, GURU and KLS1 show significant fluctuations in DROT, with values frequently exceeding the 50-60% threshold and in some cases reaching 60-70%, which corresponds to medium and large-scale disturbances as classified in this study and consistent with prior research. These elevated DROT values indicate substantial ionospheric perturbations that suggest strong coupling between seismic activity and ionospheric response, consistent with the LAIC model.

However, the relationship between epicentral distance and DROT magnitude is not straightforward. While proximity to the epicenter might be expected to produce stronger ionospheric anomalies, our observations show that some stations closer to the epicenters (e.g., ELAZ, ERGN) exhibit moderate DROT values, while stations at greater distances (e.g., ANTE, KLS1) display more pronounced disturbances. This spatial complexity suggests that ionospheric responses to seismic activity are influenced by multiple factors including regional ionospheric structure, geomagnetic conditions, local tectonic characteristics and the propagation mechanisms of Acoustic-Gravity Waves and electromagnetic perturbations. These observations underscore the importance of spatial monitoring through a dense GNSS station network to effectively capture the complex spatial patterns of pre-seismic and co-seismic ionospheric signals.

The temporal pattern reflects a clear build-up of ionospheric activity leading up to the earthquake, followed by a peak on the earthquake day. Such a trend aligns with previous findings that pre-seismic ionospheric anomalies intensify in the final 1-2 days before an event. The observed post-seismic persistence of disturbances, discussed elsewhere in the manuscript, further validates the sustained ionospheric impact of seismic processes. Overall, the data in Figure 4 support the temporal predictability of seismic-related ionospheric disturbances, reinforcing the potential of DROT-based monitoring for earthquake precursor detection and early warning applications.

4. CONCUSION

This study presents a detailed analysis of ionospheric disturbances before and during the 2023 Kahramanmaraş earthquakes using IONOLAB-TEC data estimated from a dense network of TNPGN-Active GNSS stations. The DROT algorithm is employed as a robust tool to detect and quantify ionospheric anomalies over multiple temporal scales. The findings reveal that ionospheric perturbations are not confined to a single temporal window but evolved progressively in the days leading up to the seismic events, culminating in large-scale disturbances on the day of the earthquakes.

The spatio-temporal analysis has demonstrated that DROT values increase notably within 1–2 days prior to the earthquakes, with peak values exceeding 60%, indicating large-scale ionospheric disturbances. The station-by-day matrix presented in Figure 5 confirms that anomalous DROT activity becomes consistently detectable approximately three days before the event, with ANTE recording the highest value of 70% on the earthquake day. Stations located in close proximity to the epicenters exhibit the highest DROT levels overall; however, the scatter analysis in Figure 6 reveals that epicentral distance alone is not a reliable predictor of ionospheric response magnitude, as stations such as HAT2 and ADY1 exhibit elevated responses despite their greater distance from the epicenter. These results may support the hypothesis of LAIC, wherein stress accumulation in the Earth's crust triggers atmospheric and ionospheric responses through mechanisms such as Radon gas emission, electromagnetic perturbations and Acoustic-Gravity Waves.

Comparison with a geomagnetically and seismically quiet reference day has confirmed that the observed DROT anomalies are not attributable to solar or geomagnetic activity, thus reinforcing the seismic origin of the disturbances. This distinction is further supported by the station-by-station analysis presented in Figure 7, which demonstrates a systematic and consistent elevation of mean pre-seismic DROT values relative to the quiet day baseline across the majority of stations. The progressive increase in DROT values and their spatial clustering in the vicinity of the epicenter collectively suggest that DROT-based TEC monitoring constitutes a reliable and physically interpretable method for detecting earthquake-related ionospheric anomalies. The convergence of temporal, spatial and comparative evidence presented in this study strengthens the case for seismo-ionospheric coupling as a reproducible physical phenomenon rather than a statistical artifact.

In conclusion, this study provides empirical evidence for the utility of multi-station ionospheric monitoring through DROT analysis in advancing our understanding of seismic-ionospheric interactions. The findings contribute to the growing body of research on earthquake precursors and support the feasibility of integrating ionospheric TEC data into operational early warning frameworks. The Kahramanmaraş earthquake sequence, as one of the most destructive seismic events of recent decades, represents a particularly valuable case study for the international earthquake precursor community and the results presented here are expected to facilitate comparative analyses with other major seismic events worldwide. Future work should focus on expanding the dataset to include additional global earthquake case studies of varying magnitudes and tectonic settings, incorporating post-seismic ionospheric analysis, applying statistical significance testing to DROT anomaly detection and integrating complementary geophysical and atmospheric parameters such as radon flux, atmospheric electric field variations and crustal deformation data to develop a more robust and comprehensive earthquake forecasting framework.

CONFLICT OF INTEREST

The authors declare that they have no known competing financial interests or personal relationships that could have appeared to influence the work reported in this paper.

AUTHOR CONTRIBUTION

Seçil KARATAY: Defining the Conceptual and/or Design Processes of the Study, Management of the Conceptual and/or Design Processes of the Study, Data Analysis and Interpretation, Creating the Article Draft, Critical Examination of Intellectual Content, Final Approval and Full Responsibility. Feza ARIKAN: Defining the Conceptual and/or Design Processes of the Study, Management of the Conceptual and/or Design Processes of the Study, Data Analysis and Interpretation, Creating the Article Draft, Critical Examination of Intellectual Content, Final Approval and Full Responsibility. Eren ÇELIK: Data Collection, Data Analysis and Interpretation, Creating the Article Draft, Critical Examination of Intellectual Content, Final Approval and Full Responsibility. Ömer Faruk TUTAR: Data Collection, Data Analysis and Interpretation, Creating the Article Draft, Critical Examination of Intellectual Content, Final Approval and Full Responsibility.

REFERENCES

1. Arikan, F., Erol, C. B. and Arikan, O. (2003). Regularized estimation of vertical total electron content from Global Positioning System data. *Journal of Geophysical Research: Space Physics, 108*(A12), 1-12. doi:10.1029/2002JA009605

2. Arikan, F., Erol, C. B. and Arikan, O. (2004). Regularized estimation of vertical total electron content from GPS data for a desired time period. *Radio Science, 39*(6), 1-10. doi:10.1029/2004RS003061

3. Basu, S., Basu, S., Valladares, C. E., Yeh, H.-C., Su, S.-Y. and et al. (2001). Ionospheric effects of major magnetic storms during the International Space Weather Period of September and October 1999: GPS observations, VHF/UHF scintillations and in situ density structures at middle and equatorial latitudes. *Journal of Geophysical Research: Space Physics, 106*(A12), 30389-30413. doi:10.1029/2001JA001116

4. Budak, C., Karatay, S., Erken, F. and Cinar, A. (2024). Classification of the Ionospheric Disturbances Caused by Geomagnetic and Seismic Activity with K-Nearest Neighbors Algorithm. *Wireless Personal Communications , 134*, 1551–1569. doi:10.1007/s11277-024-10965-z

5. Cherniak, I., Zakharenkova, I. and Krankowski, A. (2014). Approaches for modeling ionosphere irregularities based on the TEC rate index. *Earth, Planets and Space, 66*, 1-5. doi:10.1186/s40623-014-0165-z

6. Chowdhury, S., Bose, A. G., Das, A. and Deb, A. (2024). A study of some research work on soil radon concentration and ionospheric total electron content as earthquake precursors. *Journal of Radioanalytical and Nuclear Chemistry, 333*, 1633–1659. doi:10.1007/s10967-024-09409-6

7. Davies, K. and Baker, D. M. (1965). Ionospheric effects observed around the time of the Alaskan earthquake of March 28, 1964. *Journal of Geophysical Research: Space Physics, 70*(9), 2251-2253. doi:10.1029/JZ070i009p02251

8. Efendi, E. and Arikan, F. (2017). A fast algorithm for automatic detection of ionospheric disturbances: DROT. *Advances in Space Research, 59*(12), 2923-2933. doi:10.1016/j.asr.2017.03.018

9. Fejer, B., Farley, D., Woodman, R. and Calderon, C. (1979). Dependence of equatorial F region vertical drifts on season and solar cycle. *Journal of Geophysical Research: Space Physics, 84*(A10), 5792-5796. doi:10.1029/JA084iA10p05792

10. GFZ. (1992). *GFZ Helmholtz Centre for Geosciences*. Retrieved 05 5, 2026, from https://www-app3.gfz-potsdam.de/kp_index/Kp_ap_since_1932.txt

11. Guo, J., Yu, H., Li, W., Liu, X., Kong, Q. and Zhao, C. (2017). Total Electron Content Anomalies Before Mw 6.0+ Earthquakes in the Seismic Zone of Southwest China Between 2001 and 2013. *Journal of Testing and Evaluation, 45*(1), 131-139 . doi:10.1520/JTE20160032

12. IONOLAB. (2007). *Ionosphere Research Laboratory*. Retrieved 05 5, 2026, from www.ionolab.org

13. Jones, R. M., Ostrovsky, L. A. and Bedard, A. J. (2017). Ionospheric effects of magneto-acoustic-gravity waves: Dispersion relation. *Journal of Atmospheric and Solar-Terrestrial Physics, 159*, 7-22. doi:10.1016/j.jastp.2017.04.004

14. Kaladze, T., Pokhotelov, O., Shah, H., Khan, M. and Stenflo, L. (2008). Acoustic-gravity waves in the Earth's ionosphere. *Journal of Atmospheric and Solar-Terrestrial Physics, 70*(13), 1607-1616. doi:10.1016/j.jastp.2008.06.009

15. Karatay, S. (2020). Detection of the ionospheric disturbances on GPS-TEC using Differential Rate Of TEC (DROT) algorithm. *Advances in Space Research, 65*(10), 2372-2390. doi:10.1016/j.asr.2020.01.042

16. Karatay, S. and Gul, S. E. (2023). Prediction of GPS-TEC on Mw > 5 Earthquake Days Using Bayesian Regularization Backpropagation Algorithm. *IEEE Geoscience and Remote Sensing Letters, 20*, 1-5. doi:10.1109/LGRS.2023.3262028

17. Karatay, S., Arikan, F. and Arikan, O. (2010). Investigation of total electron content variability due to seismic and geomagnetic disturbances in the ionosphere. *Radio Science, 45*(5), 1-12. doi:10.1029/2009RS004313

18. Karatay, S., Arikan, F. and Pirti, A. (2025a). Spatio-temporal evaluation of ionospheric disturbances before, during and after earthquakes using differential rate of TEC (DROT) from GPS measurements. *Environmental Earth Sciences, 84*, 1-15. doi:10.1007/s12665-025-12216-1

19. Karatay, S., Cinar, A., and Arikan, F. (2017). Ionospheric responses during equinox and solstice periods over Turkey. *Advances in Space Research, 60*(9), 1958-1967. doi:10.1016/j.asr.2017.07.038

20. Karatay, S., Avci, S. and Bayram, B. (2025b). LSTM-Based One-Day-Ahead Prediction of Ionospheric TEC Variations Associated with Major Earthquake Events in Japan and China. *Journal of Advanced Applied Sciences, 4(1-2)*, 51-66. doi: 10.61326/jaasci.v4i1-2.432

21. Karatay, S., Arikan, F. and Arikan, O. (2026). Spectral tracks in the ionosphere: Fast Fourier Transform analysis of seismo-ionospheric coupling through GPS Total Electron Content variations. *Tectonophysics, 933*, 1-26. doi: 10.1016/j.tecto.2026.231240

22. Karpov, I. V., Kshevetsky, S. P., Borchevkina, O. P., Radievsky, A. V. and Karpov, A. I. (2016). Disturbances of the upper atmosphere and ionosphere caused by acoustic-gravity wave sources in the lower atmosphere. *Russian Journal of Physical Chemistry B , 10*, 127–132. doi:10.1134/S199079311601005X

23. Kil, H., Paxton, L. J., Pi, X., Hairston, M. R. and Zhang, Y. (2003). Case study of the 15 July 2000 magnetic storm effects on the ionosphere-driver of the positive ionospheric storm in the winter hemisphere. *Journal of Geophysical Research: Space Physics, 108*(A11), 1-22. doi:10.1029/2002JA009782

24. Kintner, P. M., Ledvina, B. M. and Paula, E. R. (2007). GPS and ionospheric scintillations. *Space Weather, 5*(9), 1-23. doi:10.1029/2006SW000260

25. Koroglu, M., and Arikan, F. (2020). Spatio-temporal analysis of ionospheric disturbances for ground based augmentation systems over a midlatitude region. *Advances in Space Research, 65*(9), 2099-2118. doi:10.1016/j.asr.2019.10.024

26. Lastovicka, J. (2009). Lower ionosphere response to external forcing: A brief review. *Advances in Space Research, 43*(1), 1-14. doi:10.1016/j.asr.2008.10.001

27. Lean, J. L., White, O. R., Livingston, W. C. and Picone, J. M. (2001). Variability of a composite chromospheric irradiance index during the 11-year activity cycle and over longer time periods. *Journal of Geophysical Research: Space Physics, 106*(A6), 10645-10658. doi:10.1029/2000JA000340

28. Leonard, R. S. and Jr, R. A. (1965). Observation of ionospheric disturbances following the Alaska earthquake. *Journal of Geophysical Research, 70*(5), 1250-1253. doi:10.1029/JZ070i005p01250

29. Liu, J. Y., Chen, Y. I., Chen, C. H., Liu, C. Y., Chen, C. Y. and et al. (2009). Seismoionospheric GPS total electron content anomalies observed before the 12 May 2008 Mw7.9 Wenchuan earthquake. *Journal of Geophysical Research: Space Physics, 114*(A4), 1-10. doi:10.1029/2008JA013698

30. Liu, J., Huang, J. and Zhang, X. (2014). Ionospheric perturbations in plasma parameters before global strong earthquakes. *Advances in Space Research, 53*(5), 776-787. doi:10.1016/j.asr.2013.12.029

31. Lundstedt, H., Liszka, L. and Lundin, R. (2005). Solar activity explored with new wavelet methods. *Annales Geophysicae, 23*(4), 1505–1511. doi:10.5194/angeo-23-1505-2005

32. Mannucci, A. J., Wilson, B. D., Yuan, D. N., Ho, C. H., Lindqwister, U. J. and Runge, T. F. (1998). A global mapping technique for GPS-derived ionospheric total electron content measurements. *Radio Science, 33*(3), 565-582. doi:10.1029/97RS02707

33. Moore, T. E., Peterson, W. K., Russell, C. T., Chandler, M. O., Collier, M. R. and et al. (1999). Ionospheric mass ejection in response to a CME. *Geophysical Research Letters, 26*(15), 2339-2342. doi:10.1029/1999GL900456

34. Moussas, X., Polygiannakis, J., Preka-Papadema, P. and Exarhos, G. (2005). Solar cycles: A tutorial. *Advances in Space Research, 35*(5), 725-738. doi:10.1016/j.asr.2005.03.148

35. Namgaladze, A. A., Klimenko, M. V., Klimenko, V. V. and Zakharenkova, I. E. (2009). Physical mechanism and mathematical modeling of earthquake ionospheric precursors registered in total electron content. *Geomagnetism and Aeronomy, 49*, 252–262. doi:10.1134/S0016793209020169

36. Nayir, H., Arikan, F., Arikan, O. and Erol, C. B. (2007). Total Electron Content Estimation with Reg-Est. *Journal of Geophysical Research: Space Physics, 112*(A11), 1-11. doi:10.1029/2007JA012459

37. Omori, Y., Yasuoka, Y., Nagahama, H., Kawada, Y., Ishikawa, T., Tokonami, S. and Shinogi, M. (2007). Anomalous radon emanation linked to preseismic electromagnetic phenomena. *Natural Hazards and Earth System Sciences, 7*(5), 629–635. doi:10.5194/nhess-7-629-2007

38. Ondoh, T. (2009). Investigation of precursory phenomena in the ionosphere, atmosphere and groundwater before large earthquakes of M > 6.5. *Advances in Space Research, 43*(2), 214-223. doi:10.1016/j.asr.2008.04.003

39. Pap, J., Tobiska, W. K. and Bouwer, S. D. (1990). Periodicities of solar irradiance and solar activity indices, I. *Solar Physics, 129*, 165–189. doi:10.1007/BF00154372

40. Paul, K. S., Rafi, M. H., Haralambous, H. and Mostafa, M. G. (2024). Correlation of Rate of TEC Index and Spread F over European Ionosondes. *Atmosphere, 15*(3), 1-17. doi:10.3390/atmos15030331

41. Pulinets, S. (1998). Seismic activity as a source of the ionospheric variability. *Advances in Space Research, 27*(6), 903-906. doi:10.1016/S0273-1177(98)00121-5

42. Pulinets, S. A. and Legen'ka, A. D. (2003). Spatial–Temporal Characteristics of Large Scale Disturbances of Electron Density Observed in the Ionospheric F-Region before Strong Earthquakes. *Cosmic Research, 41*, 221–230. doi:10.1023/A:1024046814173

43. Pulinets, S. and Ouzounov, D. (2011). Lithosphere–Atmosphere–Ionosphere Coupling (LAIC) model – An unified concept for earthquake precursors validation. *Journal of Asian Earth Sciences, 41*(4/5), 371-382. doi:10.1016/j.jseaes.2010.03.005

44. Rapoport, Y., Gotynyan, O., Ivchenko, V., Kozak, L. and Parrot, M. (2004). Effect of acoustic-gravity wave of the lithospheric origin on the ionospheric F region before earthquakes. *Physics and Chemistry of the Earth, Parts A/B/C, 29*(4-9), 607-616. doi:10.1016/j.pce.2003.10.006

45. Ridley, A., Zeeuw, D. D., Manchester, W. and Hansen, K. (2006). The magnetospheric and ionospheric response to a very strong interplanetary shock and coronal mass ejection. *Advances in Space Research, 38*(2), 263-272. doi:10.1016/j.asr.2006.06.010

46. Sezen, U., Arikan, F., Arikan, O., Ugurlu, O. and Sadeghimorad, A. (2013). Online, automatic, near-real time estimation of GPS-TEC: IONOLAB-TEC. *Space Weather, 11*(5), 297-305. doi:10.1002/swe.20054

47. Shah, M., Ahmed, A., Ehsan, M., Khan, M., Tariq, M. A., Calabia, A. and Rahman, Z. ur. (2020). Total electron content anomalies associated with earthquakes occurred during 1998–2019. *Acta Astronautica, 175*, 268-27. doi:10.1016/j.actaastro.2020.06.005

48. Sun, L., Wan, W., Ding, F. and Mao, T. (2007). Gravity wave propagation in the realistic atmosphere based on a three-dimensional transfer function model. *Annales Geophysicae, 25*(9), 1979–1986. doi:10.5194/angeo-25-1979-2007

49. Swamy, K. C., Devanaboyina, V. R., Nallagarla, R., Shaik, T. A. and Turpati, S. (2024). Correlation between rate of TEC index and positioning error during solar flares and geomagnetic storms using navigation with Indian constellation receiver measurements. *Journal of Applied Geodesy, 19*(1), 49-58. doi:10.1515/jag-2024-0022

50. Tete, S., Otsuka, Y., Zahra, W. K. and Mahrous, A. (2024). Leveraging machine learning techniques and GPS measurements for precise TEC rate predictions. *GPS Solutions , 28*, 1-16. doi:10.1007/s10291-024-01652-4

51. USGS. (1879). *United States Geological Survey*. Retrieved 05 05, 2026, from https://www.usgs.gov/

52. WDC. (1957). *WDC for Geomagnetism, Kyoto*. Retrieved 05 05, 2026, from https://wdc.kugi.kyoto-u.ac.jp///dstae///wwwtmp/WWW_dstae03340870.dat

53. Yasyukevich, Y., Astafyeva, E., Padokhin, A., Ivanova, V., Syrovatskii, S. and Podlesnyi, A. (2018). The 6 September 2017 X-Class Solar Flares and Their Impacts on the Ionosphere, GNSS and HF Radio Wave Propagation. *Space Weather, 16*(8), 1013-1027. doi:10.1029/2018SW001932

54. Zakharenkova, I., Shagimuratov, I., Tepenitzina, N. and Krankowski, A. (2008). Anomalous modification of the ionospheric total electron content prior to the 26 September 2005 Peru earthquake. *Journal of Atmospheric and Solar-Terrestrial Physics, 70*(15), 1919-1928. doi:10.1016/j.jastp.2008.06.003